Asian Journal of Chemistry; Vol. 38, No. 9 (2026), 2314-2322
ASIAN JOURNAL OF CHEMISTRY
https://doi.org/10.14233/ajchem.2026.36471

Comparative Photocatalytic Degradation of Alizarin Red S Dye using Cobalt-Doped TiO_2 under UV, Visible and Solar Light Irradiation

NIKITA S. GUPTA[1,2,*] and SUSMITA A. MANDAVGANE[3]

[1]Department of Chemistry, Lady Amritbai Daga College & Smt. Ratnidevi Purohit College, Nagpur-440010, India
[2]Department of Chemistry, Rashtrasant Tukadoji Maharaj Nagpur University, Nagpur-440033, India
[3]Department of Chemistry, DRB Sindhu Mahavidyalaya, Nagpur-440017, India

*Corresponding author: E-mail: nikitag7496@gmail.com

Received: 20 May 2026 *Accepted*: 25 July 2026 *Published online*: 5 September 2026 AJC-22459

Titanium dioxide (TiO_2) is a widely studied photocatalyst, although its broad band gap restricts its response mainly to the ultraviolet region. This study investigates the effect of cobalt doping on the optical properties and photocatalytic activity of TiO_2 under ultraviolet (UV), visible and solar irradiation. Co-doped TiO_2 containing 0.5 mol% Co was synthesized by the sol–gel method. The crystal structure, morphology, particle size and elemental composition were examined by X-ray diffraction (XRD), scanning electron microscopy (SEM), transmission electron microscopy (TEM), selected-area electron diffraction (SAED) and energy-dispersive X-ray spectroscopy (EDX). Optical absorption characteristics were evaluated by UV-visible diffuse reflectance spectroscopy (DRS) and the band gap energy was estimated from Tauc plots. The photocatalytic activity of the materials was evaluated using Alizarin dye as a model pollutant under UV, visible and solar irradiation, with the degradation kinetics analyzed using a pseudo-first-order model. XRD analysis confirmed the formation of highly crystalline, single-phase anatase TiO_2. TEM images revealed nearly spherical nanoparticles with particle sizes of approximately 30-40 nm, while SAED patterns were consistent with the crystalline anatase structure. EDX analysis confirmed the presence of Co and TiO_2 constituents without detectable extraneous elements. Co doping reduced the optical band gap from 3.2 eV for pristine TiO_2 to 2.0 eV for Co-doped TiO_2, extending the light absorption toward the visible region. After 60 min of irradiation, Alizarin red S (ARS) degradation reached 73.53%, 48.44% and 63.46% under UV, visible and solar light, respectively, with corresponding pseudo-first-order rate constants of 0.01819, 0.01073 and 0.01608 min^{-1}. The reduced band gap and enhanced reaction kinetics under visible and solar irradiation establish Co-doped TiO_2 as an effective photocatalyst for light-assisted wastewater treatment.

Keywords: Alizarin dye, Degradation, Band gap reduction, Doped TiO_2, Photocatalysis, Sol gel synthesis, UV–Vis DRS.

INTRODUCTION

The discharge of inadequately treated industrial wastewater is a major source of persistent organic pollution in aquatic ecosystems. Dye-containing effluents are particularly concerning due to the extensive use of synthetic dyes in textile, leather, paper, plastic, pharmaceutical, food and cosmetic industries. Their chemical stability and resistance to biodegradation enable persistence in water, while even low concentrations can reduce light penetration, disrupt photosynthesis and adversely affect aquatic organisms. Moreover, several synthetic dyes and their degradation products exhibit toxic, mutagenic, genotoxic and carcinogenic potential [1-3]. The treatment of dye-bearing wastewater consequently requires processes capable of not only transferring the contaminants from one phase to another but also destroying their molecular structures [4].

Alizarin Red S (ARS), an anthraquinone dye containing hydroxyl, carbonyl and sulphonate groups, exhibits intense colouration, chemical stability and strong interactions with aqueous and solid interfaces. Its persistence and resistance to conventional degradation make it a suitable model pollutant for evaluating advanced oxidation processes. Previous studies [5-7] have demonstrated effective photocatalytic degradation of ARS using TiO_2 and other semiconductor catalysts, with degradation strongly influenced by dye-catalyst interactions and irradiation conditions Visible-light responsive photocatalysts have gained particular interest due to their potential for utilizing a larger fraction of solar radiation for removal of ARS dye [8,9].

A range of physico-chemical and biological methods has been employed for the removal of dye, including adsorption, chemical precipitation, coagulation-flocculation, membrane separation, biological treatment, ozonation, Fenton-based oxidation and electrochemical processes. Many of these techniques are effective for colour removal but may involve high chemical consumption, sludge generation, membrane fouling, energy-intensive operation or transfer of the contaminant to another phase rather than its molecular destruction [10,11]. Advanced oxidation processes (AOPs) provide a different treatment path-way through the generation of highly reactive oxygen species (ROS), such as hydroxyl radicals ($^{\bullet}OH$), superoxide radicals ($O_2^{\bullet-}$), hydroperoxyl radicals ($HO_2^{\bullet}$) and other oxidizing intermediates. These species can attack aromatic rings and other functional groups present in unruly organic molecules, initiating a sequence of oxidation reactions that can lead to smaller intermediates and under suitable conditions, mineralization to CO_2, H_2O and inorganic ions [12,13].

Among the numerous semiconductor photocatalysts investigated for water treatment, TiO_2 has received considerable attention due to its high chemical stability, relatively low toxicity, corrosion resistance, abundance and cost-effectiveness, together with its high photocatalytic activity [14]. Upon irradiation with photons possessing energy equal to or greater than its band-gap energy, TiO_2 generates photogenerated electron–hole (e^-/h^+) pairs, which can participate in a series of redox reactions leading to the degradation of organic pollutants. However, the practical application of pristine TiO_2 is largely restricted to ultraviolet (UV) irradiation due to its wide band gap (~ 3.0-3.2 eV), which limits its utilization of the visible-light region [15]. In addition, rapid recombination of photogenerated electron–hole pairs substantially decrease the availability of charge carriers for surface redox reactions, thereby limiting the photocatalytic efficiency. Achieving efficient visible-light absorption while simultaneously maintaining sufficient redox potential therefore remains a major challenge in the development of TiO_2-based photocatalysts.

To overcome these limitations, various strategies like elemental doping, have been employed to modify the electronic structure and charge-carrier dynamics of TiO_2 [16]. Incorporation of dopant ions into the TiO_2 lattice can introduce impurity levels, oxygen vacancies, or other defect states that influence charge-carrier migration and separation, suppress electron–hole recombination and potentially extend the lifetime of photogenerated carriers, thereby improving photocatalytic performance [17]. Transition-metal doping is widely investigated for modifying the electronic structure, optical absorption and charge-carrier behaviour of TiO_2. Cobalt has attracted particular attention as a dopant, since the incorporation of Co^{2+} ions into TiO_2 can introduce impurity levels and defect states that alter light absorption and photogenerated charge-carrier dynamics. The substitution of Co^{2+} for Ti^{4+} may require charge compensation through the formation of oxygen vacancies or other lattice defects; consequently, the effect of cobalt incorporation depends strongly on dopant concentration, oxidation state, crystal phase and local coordination environment [18,19]. Co-doped TiO_2 has been investigated for the degradation of organic dyes under UV and visible-light irradiation, with methylene blue and rhodamine B among the frequently selected model pollutants [20,21]. The available literature on anthraquinone dyes, particularly alizarin and alizarin red S, is comparatively limited. A systematic assessment of Co-doped TiO_2 under UV, visible and solar irradiation, coupled with an evaluation of the relationship between cobalt-induced structural and electronic modifications and photocatalytic performance, can provide a clearer understanding of its suitability for anthraquinone dye degradation.

This study aims to comparatively evaluates the photocatalytic degradation of alizarin red S (ARS) in aqueous solution using Co-doped TiO_2 nanostructures under different irradiation conditions, namely UV, visible and solar light. The study focuses on the changes in the structure, optical behaviour and electronic characteristics of TiO_2 caused by cobalt doping and relates these changes to the degradation of ARS under UV, visible and solar light.

EXPERIMENTAL

Titanium(IV) tetra-*n*-butoxide [$Ti(OBu)_4$] (Sigma-Aldrich) was used as the titanium precursor for the preparation of TiO_2 nanoparticles. Cobalt nitrate hexahydrate [$Co(NO_3)_2{\cdot}6H_2O$], Loba Chemie Pvt. Ltd., was used as the source of cobalt doping. Alizarin dye, Loba Chemie Pvt. Ltd., was chosen as the organic model pollutant for photocatalytic degradation experiments. Nitric acid and sulphuric acid were used for pH adjustment, while ethanol was used as the solvent for the preparation of samples. The reagents were all analytical reagent (AR) grades, which meant that all reagents were not required to be purified any longer. Double-distilled water was used for formulation of all aqueous solutions.

Synthesis of Co-doped TiO_2 photocatalyst: Co-doped TiO_2 nanoparticles were synthesized *via* a sol-gel method to achieve homogeneous dopant dispersion within the TiO_2 matrix. Initially, 10 mL of $Ti(OBu)_4$ was added dropwise to 40 mL of ethanol under continuous magnetic stirring and maintained for 5 min. Subsequently, 1 mL of HNO_3 was introduced slowly into the solution, followed by further stirring for 10 min to suppress the premature hydrolysis of the titanium precursor. Thereafter, an aqueous cobalt nitrate solution corresponding to 0.5 mol% Co with respect to Ti was gradually added to the sol. The Co loading of 0.5 mol% was selected based on previous studies [22] since low dopant concentrations effectively narrow the band gap of TiO_2 and improve visible-light absorption, whereas excessive dopant loading may generate charge recombination centers, which adversely affect the photocatalytic performance.

Gelation was induced by the gradual addition of 5 mL of distilled water under constant stirring. The resulting gel was aged at room temperature for 24 h to ensure complete gelation and structural stabilization. The obtained xerogel was subsequently dried at 105 ºC for 12 h to remove residual solvent and moisture. Finally, the dried xerogel was calcined at different temperatures ranging from 200 to 600 ºC for 1 h in a muffle furnace at a heating rate of 5 ºC min^{-1}. Among the calcined samples, the material treated at 500 ºC exhibited superior photocatalytic performance and was therefore selected for subsequent photocatalytic studies.

Evaluation of photocatalytic activity: The photocatalytic activity of Co-doped TiO_2 nanoparticles was evaluated by monitoring the degradation of alizarin red S (ARS) under UV, visible and natural sunlight irradiation. An aqueous ARS solution with an initial concentration of 10 mg L^{-1} was prepared and 100 mL of the solution was transferred to the photoreaction vessel. Co-doped TiO_2 photocatalyst (0.1 g) was dispersed in the dye solution and the suspension was magnetically stirred in the dark for 30 min to establish adsorption-desorption equilibrium between the photocatalyst surface and dye molecules. The equilibrated suspension was subsequently irradiated separately using natural sunlight, a visible-light LED lamp and a UV lamp operating at 365 nm. Aliquots of 5 mL were withdrawn at predetermined irradiation times of 10, 15, 30, 45, 60 and 90 min. Each aliquot was centrifuged to remove the suspended photocatalyst and the supernatant was analyzed using a UV-visible spectrophotometer. The residual ARS concentration was determined from its characteristic absorption maximum at 520 nm. The extent of photocatalytic degradation was calculated from the change in ARS concentration during irradiation. This efficiency degradation (%) was calculated by using the following equation:

$$\text{Degradation efficiency (\%)} = \frac{C_o - C_t}{C_o} \times 100 \qquad (1)$$

where C_o = initial dye concentration, C_t = dye concentration at time t.

The degradation kinetics were examined utilizing a pseudo-first-order kinetic model by plotting ln (C_o/C_t) against time to ascertain the apparent rate constant (k).

Characterization: The crystal structure of Co-doped TiO_2 nanoparticles was analyzed by X-ray diffraction (XRD, PANalytical X'Pert PRO) over 2θ = 20-80º and the crystallite size was estimated using the Scherrer equation. Lattice parameters were calculated to assess structural changes associated with Co incorporation. Morphology and particle size were examined by SEM (JEOL JSM-7600F) and TEM (JEOL JEM-2100), while EDX was used to determine elemental composition and confirm Co incorporation. Optical properties were evaluated by UV-Vis diffuse reflectance spectroscopy (DRS, Shimadzu UV-2600). The optical band gap was estimated from Tauc plots using the Kubelka-Munk function and an indirect allowed-transition model. FTIR spectroscopy was used to identify characteristic bonding and surface functional groups. During photocatalytic experiments, the residual ARS concentration was determined using a Shimadzu UV-Vis spectrophotometer (UV-1900i Plus) at 520 nm.

RESULTS AND DISCUSSION

XRD analysis: The XRD pattern of 0.5 mol% Co-doped TiO_2 nanoparticles exhibits sharp and well-defined diffraction peaks, characteristic of a highly crystalline material (Table-1). The most intense reflection appears at 2θ ≈ 25.28º, corresponding to the (101) plane of anatase TiO_2. Other prominent reflections at approximately 37.08º, 47.85º, 54.65º, 62.9º and 70.15º are assigned to the (004), (200), (105), (204) and (220) planes (Fig. 1), respectively, in accordance with the standard anatase TiO_2 pattern (JCPDS No. 21-1272). The absence of distinct diffraction peaks attributable to cobalt oxides or other secondary crystalline phases suggests that no appreciable phase segregation occurred at the investigated Co concentration. The Co species are likely incorporated into or associated with the TiO_2 lattice at a level below the detection limit of XRD. Refined lattice distortions arising from Co incorporation may not be resolved directly from the diffraction pattern, yet such structural perturbations can modify the electronic environment of TiO_2 and influence its photocatalytic behaviour. The average crystallite size was estimated from the broadening of the diffraction peaks using the Scherrer's equation [23].

TABLE-1
XRD PEAK POSITIONS, MILLER INDICES AND CRYSTALLITE SIZES OF 0.5 mol% Co-DOPED TiO_2 NANOPARTICLES

2θ (º)	Plane (*hkl*)	Crystallite size (nm)
25.28	101	18
37.08	103	18
47.85	200	19
54.65	105	17
62.90	204	18
70.15	215	17

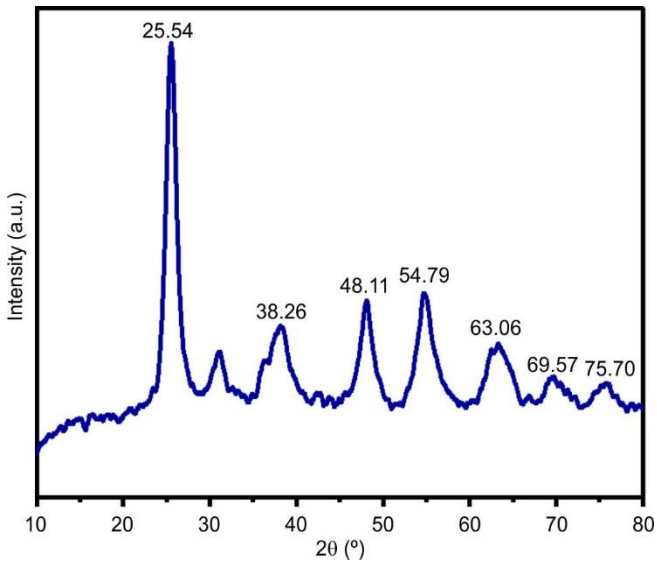

Fig. 1. XRD pattern of 0.5 mol% Co-doped TiO_2 nanoparticles showing peaks corresponding to anatase phase (JCPDS 21-1272)

$$D = \frac{K\lambda}{\beta \cos\theta} \qquad (2)$$

where K is constant, λ = wavelength of X-rays and β =Full width at half maximum (FWHM).

FTIR studies: The FTIR spectrum of the Co-doped TiO_2 photocatalyst is shown in Fig. 2. A broad band centered near 3400 cm^{-1} is assigned to the O–H stretching vibration of surface hydroxyl groups and adsorbed water molecules. Surface hydroxyl groups can participate in the generation of reactive oxygen species during photocatalytic reactions and are relevant to the surface oxidation of organic pollutants. The band at approximately 1637 cm^{-1} corresponds to the H–O–H bending vibration of molecularly adsorbed water. The lower-wavenumber region contains bands associated with Ti–O–Ti and Ti–O lattice vibrations. The absorption feature near 679

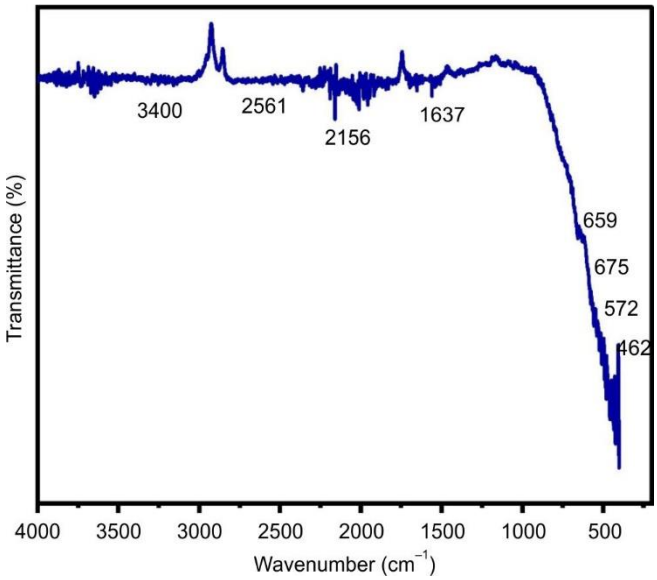

Fig. 2. FTIR spectrum of 0.5 mol% Co-doped TiO_2 catalyst

cm^{-1} can be assigned to Ti–O–Ti stretching vibrations, while the band around 670 cm^{-1} is associated with Ti–O lattice vibrations [14,24]. A shift in the band from approximately 1400 to 1384 cm^{-1} might be due to the changes occur in the local bonding environment following Co incorporation into the TiO_2 structure. Such spectral changes are consistent with modifications of the TiO_2 lattice and surface chemistry induced by cobalt species. The FTIR results, considered with the XRD analysis, support the presence of Co-modified TiO_2 without distinct vibrational features attributable to a separate cobalt oxide phase.

Morphological studies: The morphology of 0.5 mol% Co-doped TiO_2 nanoparticles was examined by SEM and TEM, as shown in Fig. 3. The SEM image (Fig. 3a) displays predominantly spheroidal and granular particles with a rough surface texture and noticeable agglomeration. Such aggregation is commonly associated with the high surface energy and interparticle interactions of nanosized materials. Some irregularly shaped and rod-like features are visible at higher magnification. The TEM image further confirms the nanoscale nature of the material, with nearly spherical particles having sizes in the range of 30-40 nm. The relatively rough morphology and nanoscale dimensions provide a substantial surface area and accessible active sites for interaction with ARS during photocatalytic degradation [25].

The EDX spectrum (Fig. 3b) contains characteristic signals of titanium, oxygen and cobalt, which confirm the elemental composition of the Co-doped TiO_2 sample. Ti and O constitute the major components of the TiO_2 matrix, while the Co signal confirms the presence of the dopant. No additional elemental signals associated with detectable foreign impurities were observed within the analytical limits of EDX. The analyzed region contained 11.0 wt.% Co and 5.1 at.% Co. Since EDX provides localized elemental information, the measured Co concentration may differ from the nominal 0.5 mol% composition used during synthesis, particularly when an agglomerated region is selected for analysis. The absence of detectable extra elements confirms the compositional purity of the analyzed region.

TEM analysis: The TEM images of the Co-doped TiO_2 nanoparticles (Fig. 3c-e) provide further insight into their morphology, particle size and crystalline characteristics. The nanoparticles are predominantly spherical with a relatively

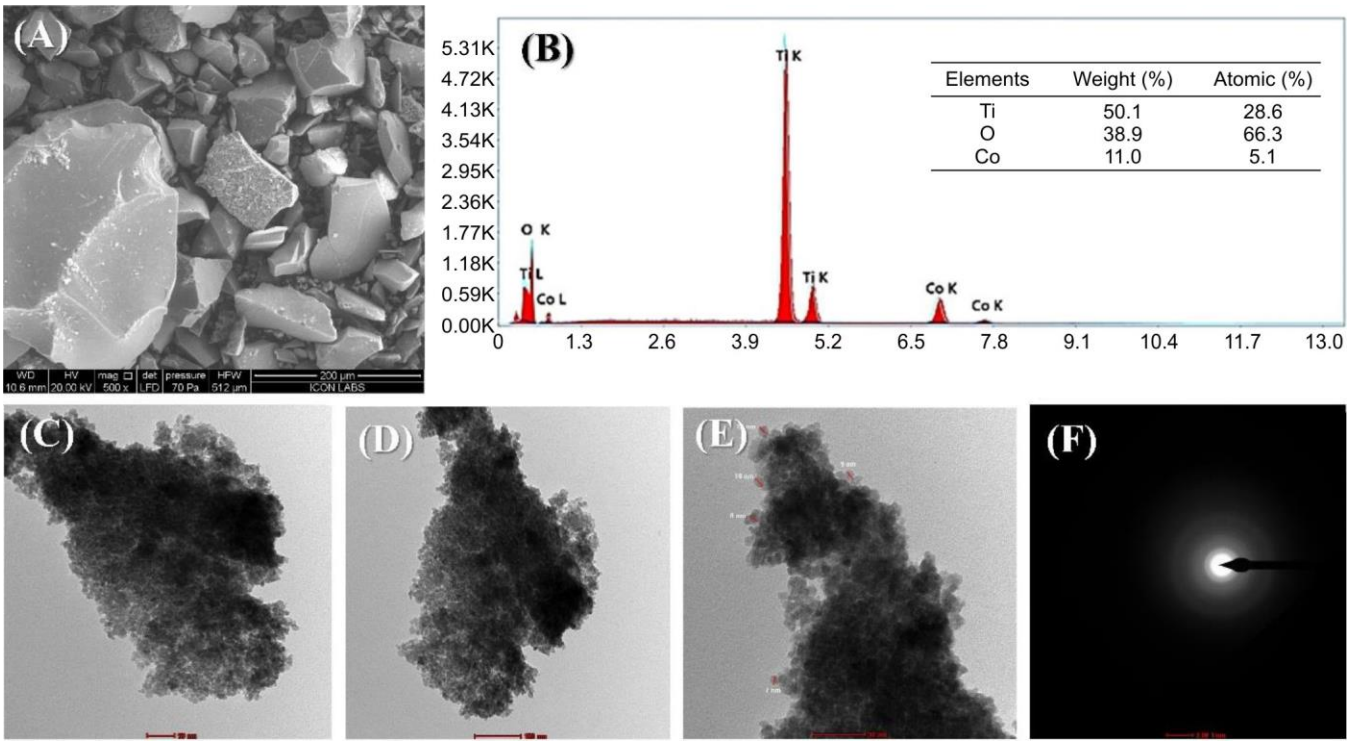

Fig. 3. SEM image of Co-doped TiO_2 (A), EDX spectrum of 0.5 mol% Co-doped TiO_2 (B), TEM images (C-E) and SAED pattern of Co-doped TiO_2 photocatalyst (F)

uniform size distribution, ranging from 30 to 40 nm in diameter. The dark contrast of the nanoparticles against the brighter background arises from differences in electron scattering within the sample. Some degree of particle agglomeration is observed, with individual nanoparticles forming larger clusters through interparticle interactions. The SAED pattern (Fig. 3f) consists of concentric diffraction rings, characteristic of a polycrystalline structure. The well-defined rings are consistent with the crystalline anatase phase of TiO_2 and agree with the XRD results.

UV-Vis DRS studies: The UV-Vis diffuse reflectance spectra (DRS) of pristine and Co-doped TiO_2 were recorded to evaluate the effect of cobalt incorporation on their optical response (Table-2). Incorporation of Co causes a pronounced shift of the absorption edge toward longer wavelengths compared with pristine TiO_2 (Fig. 4a). This red shift extends the optical response into the visible region and is accompanied by a reduction in the apparent band-gap energy. The modified absorption behaviour can be associated with Co-related electronic states introduced within the TiO_2 band structure, which facilitate lower-energy optical transitions. The enhanced absorption in the visible region is relevant to the utilization of a broader portion of the solar spectrum during photocatalytic reactions. The optical band-gap energies were estimated from Tauc plots (Fig. 4b) using the Kubelka-Munk function and assuming an indirect allowed transition, which is commonly applied to anatase TiO_2. The relationship can be expressed as

$$(\alpha h\nu)^{1/2} = A(h\nu - E_g) \quad (3)$$

where α = absorption coefficient, $h\nu$ = photon energy, E_g = band gap energy.

The optical band-gap energy of pristine TiO_2 was estimated to be ~3.2 eV, which is consistent with the anatase phase. Upon Co incorporation, the band-gap energy decreased markedly to approximately 2.0 eV. This reduction can be associated with Co-induced impurity states and defect levels within the TiO_2 electronic structure, which provide additional electronic transitions at lower photon energies. The modified electronic structure extends the optical response toward the visible region and can facilitate higher utilization of visible photons during photocatalytic reactions [24].

Photocatalytic degradation: The photocatalytic activity of pristine TiO_2 and 0.5 mol% Co-doped TiO_2 was evaluated by monitoring the degradation of ARS under UV, visible and natural sunlight irradiation. The blank experiments exhibited 15.0% degradation under UV light, 8.8% under solar irradiation and negligible degradation under visible light after 60 min. Pristine TiO_2 achieved approximately 54.0% degradation under UV irradiation and 37.0% under solar irradiation, while no appreciable degradation was observed under visible

TABLE-2
COMPARISON OF OPTICAL BAND GAP ENERGIES AND ABSORPTION EDGE WAVELENGTHS OF PURE TiO_2, 0.5 MOL% Co-DOPED TiO_2 AND PREVIOUSLY REPORTED CATALYSTS

Sample	Band gap (eV)	Transition type	Absorption edge (nm)	Ref.
Co-doped TiO_2	2.90	Direct	425	[19]
Co-doped TiO_2@300	2.37	Indirect	NA	[25]
Co-doped TiO_2@400	2.51	Indirect	NA	[25]
Co-doped TiO_2@600	2.30	Indirect	NA	[25]
Co-doped TiO_2-R	2.93	Indirect	NA	[26]
Co-doped TiO_2-HT	3.03	Indirect	NA	[26]
Pure TiO_2	3.20	Indirect	387	Present study
5 mol% Co-doped TiO_2	2.00	Indirect	620	Present study

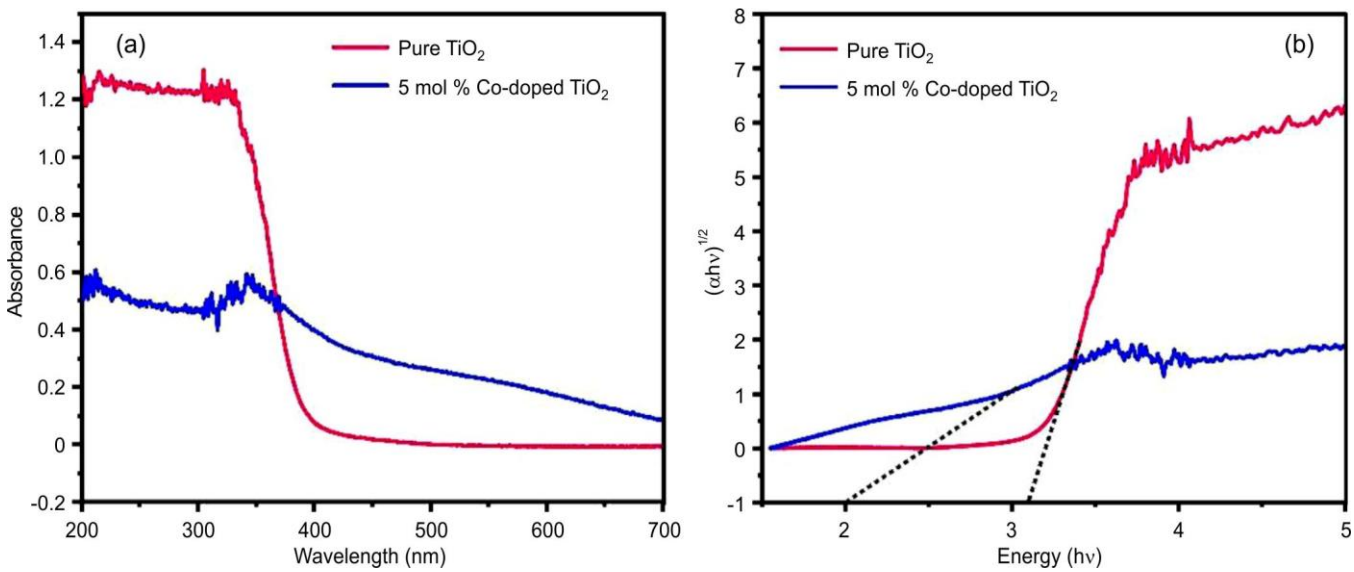

Fig. 4. (a) UV-Vis absorption spectrum of pure TiO_2 and 0.5 mol% Co-doped TiO_2 exhibiting a red shift in the absorption edge; (b) Tauc plot for band gap estimation

light within the same reaction period (Table-3). The higher activity of Co-doped TiO_2 under all three irradiation conditions confirms the beneficial role of cobalt incorporation in modifying the photocatalytic response of TiO_2.

TABLE-3
PHOTOCATALYTIC ARS DYE (10 mg/L)
DEGRADATION ACTIVITY OF CATALYSTS

Catalyst	Degradation efficiency of Alizarin dye (%)			
	Dark	UV	Visible	Solar
Blank (No catalyst)	0	15.0	0	08.8
TiO_2	0	54.4	0	32.7
0.25 mol% Co-doped TiO_2	0	61.5	28.1	47.5
0.5 mol% Co-doped TiO_2	0	73.5	48.4	63.4
1 mol% Co-doped TiO_2	0	70.4	37.4	55.3

Reaction condition: 100 mL Alizarine dye solution (10 mg/L), 0.1 g catalyst, 60 min.

The 0.5 mol% Co-doped TiO_2 catalyst achieved 73.53% degradation of ARS under UV irradiation after 60 min, representing the highest activity among the investigated irradiation conditions (Table-3). The pronounced degradation during the initial 30 min of UV exposure can be associated with efficient photo-excitation of TiO_2 and the generation of electron–hole pairs, which participate in the surface oxidation and reduction reactions.

Under visible-light irradiation, the Co-doped TiO_2 catalyst achieved 48.44% degradation of ARS within 60 min. The visible-light response is consistent with the reduced optical band gap observed after Co incorporation, which enables absorption of lower-energy photons and facilitates photocatalytic reactions beyond the intrinsic UV response of TiO_2. Solar irradiation resulted in 63.46% degradation after 60 min (Table-3), reflecting the combined contribution of the UV and visible components of sunlight. The activity observed under solar and visible irradiation confirms that Co modification extends the photocatalytic response of TiO_2 toward a broader spectral range. The comparative degradation profiles are shown in Fig. 5.

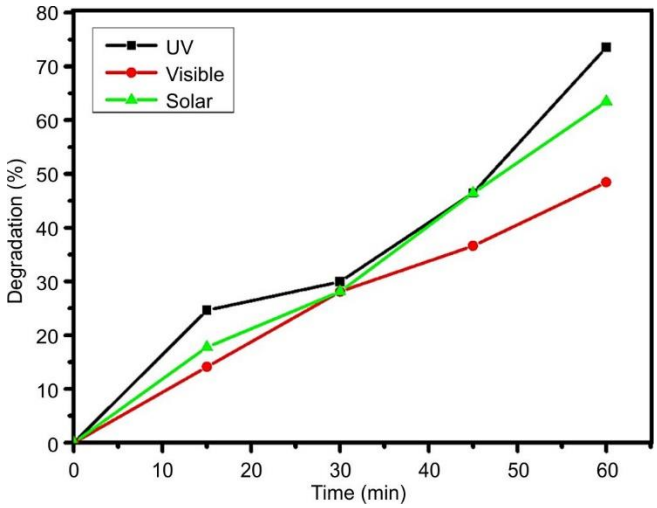

Fig. 5. Photocatalytic degradation of ARS dye over Co-doped TiO_2 exposed to UV, visible and solar light

Kinetic studies: The photodegradation of ARS dye by the synthesized Co-doped TiO_2 nanoparticles follows pseudo-first kinetic order kinetics under all the light sources (Table-4). The degradation rate kinetics for all the light sources obey a pseudo-first-order reaction model (eqn. 4):

$$\ln\left(\frac{C_o}{C}\right) = kt \qquad (4)$$

where C_o is the initial dye concentration, C is the concentration at time t, k is the pseudo-first-order rate constant and t is the irradiation time (Fig. 6a). The UV-irradiated system exhibited the steepest slope and the highest apparent rate constant, consistent with the more efficient generation of photogenerated charge carriers under 365 nm irradiation. Solar irradiation gave an intermediate slope, while visible irradiation resulted in the lowest slope and rate constant, corresponding to slower ARS degradation. The concentration plots shown in Fig. 6b follow the same trend, with a more rapid decrease in (C/C_o) under UV irradiation than under solar and visible light.

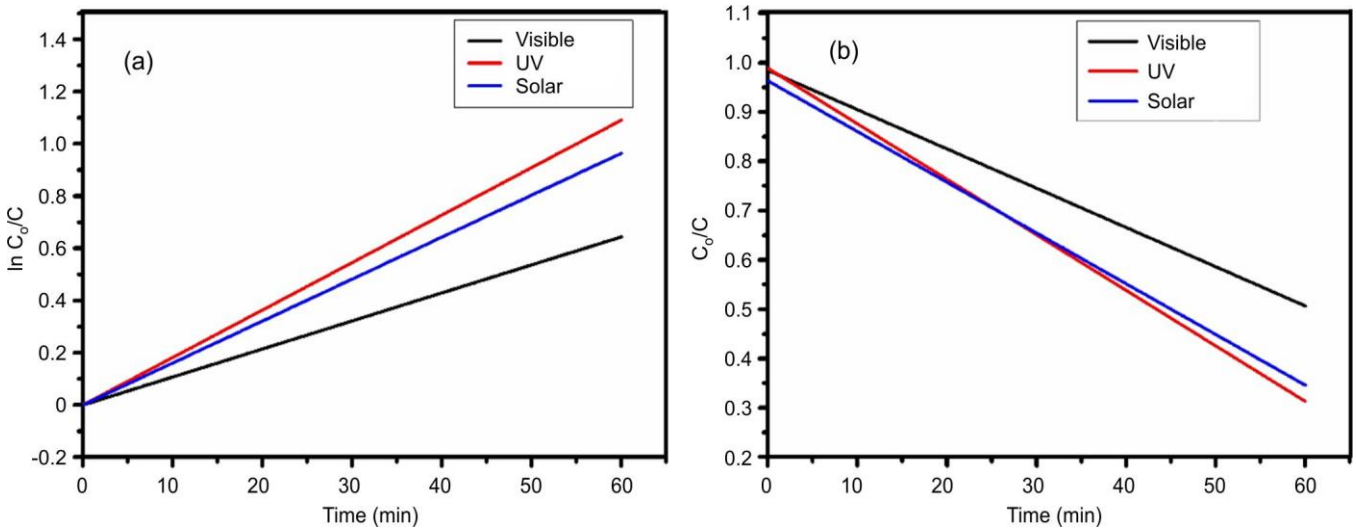

Fig. 6. (a) Pseudo-first-order kinetic graphs ($\ln C_o/C$ *vs.* time) and (b) concentration decay profiles (C/C_o *versus* time) for the photocatalytic breakdown of ARS dye on Co-doped TiO_2 under UV, visible and solar light irradiation

TABLE-4
KINETIC RATE CONSTANTS AND DEGRADATION EFFICIENCY OF ARS DYE USING CO-DOPED TiO_2 PHOTOCATALYSTS

Dye	Doped TiO_2	Condition of light	k (min^{-1})	Degradation (%)
Alizarin dye	Co-doped TiO_2	Visible	0.01073	48.44
		UV	0.01819	73.53
		Solar	0.01608	63.46

The kinetic results establish the order of photocatalytic activity as UV > solar > visible irradiation. Although UV light provided the highest degradation rate, Co incorporation enabled appreciable photocatalytic activity under visible and solar irradiation. This extended photoresponse is associated with the modified electronic structure of Co-doped TiO_2 and supports its application in solar-light-assisted treatment of dye contaminated wastewater [27].

Comparative studies: Previous studies [28-30] have established that the incorporation of 3*d*-transition metal ions can modify the electronic structure of TiO_2 by introducing dopant-related states within the band-gap region. In present study, the incorporation of Co decreased the optical band-gap energy from 3.2 eV for pristine TiO_2 to approximately 2.0 eV for Co-doped TiO_2. The narrowing of the apparent band gap can be associated with Co-related 3*d* electronic states and defect levels introduced into the TiO_2 band structure, which facilitate lower energy electronic transitions [31]. This modification extends the optical response of TiO_2 toward the visible region and increases the fraction of incident radiation capable of initiating photocatalytic reactions. Compared with previously reported modified TiO_2 catalysts summarized in Table-5, the higher ARS degradation achieved by Co-doped TiO_2 in the present study indicates that Co incorporation more effectively enhances visible-light absorption and facilitates the generation and utilization of photogenerated charge carriers.

Proposed mechanism: Under irradiation with photon energy equal to or higher than the modified band gap, electrons are excited from the valence band to the conduction band, generating photo-generated electron–hole pairs. The photo-generated electrons can reduce dissolved O_2 to form superoxide radicals ($O_2^{\bullet-}$), while valence-band holes can react with surface H_2O or hydroxyl groups to generate hydroxyl radicals ($^{\bullet}OH$). These reactive oxygen species, together with photo-generated holes, attack the adsorbed ARS molecules and initiate successive oxidation reactions. The proposed photocatalytic reaction pathway for Co-doped TiO_2 can be represented by the following reactions:

$$Co@TiO_2 \xrightarrow{hv} Co_{3d}^{2+}(h^+) + TiO_2(e^-)$$

$$OH^- + h^+ \longrightarrow OH^{\bullet}$$

$$O_2 + e^- \longrightarrow O_2^{\bullet-}$$

$$O_2^{\bullet-} + H^+ \longrightarrow HO_2^{\bullet}$$

$$HO_2^{\bullet} + e^- \longrightarrow HO_2^-$$

$$HO_2^- + H^+ \longrightarrow H_2O_2$$

$$H_2O_2 + e^- \longrightarrow OH^- + HO^{\bullet}$$

$$ARS + HO^{\bullet} \longrightarrow CO_2 + H_2O + \text{Simple molecules}$$

Upon irradiation of the Co-doped TiO_2 photocatalyst with photons having energy equal to or higher than its optical band gap ($h\nu \geq E_{bg}$), electrons are excited from the valence band (VB) to the conduction band (CB), generating photogenerated electron-hole pairs. The Co-related electronic states introduced into the TiO_2 band structure can participate in charge trapping and transfer processes, reducing the probability of rapid electron-hole recombination. The photogenerated electrons at the CB can react with adsorbed molecular oxygen to form superoxide radicals ($O_2^{\bullet-}$). These species can undergo subsequent protonation and redox reactions, generating other reactive oxygen species. At the same time, the photogenerated holes can oxidize surface OH^- groups or water molecules to form highly reactive hydroxyl radicals ($HO^{\bullet}$). The generated reactive species attack the adsorbed ARS molecules through successive oxidation reactions, leading to the cleavage of the anthraquinone structure and formation of smaller intermediate products, which may undergo further oxidation toward CO_2, H_2O and inorganic species [39]. This mechanism provides a plausible pathway for the enhanced ARS degradation observed with Co-doped TiO_2 under UV, visible and solar irradiation and can be explained through Fig. 7.

Conclusion

Sol-gel synthesized 0.5 mol% Co-doped TiO_2 nanoparticles exhibited enhanced photocatalytic activity toward Alizarin Red S (ARS) under UV, visible and solar irradiation. Co incorporation decreased the optical band-gap energy from 3.2 eV for pristine TiO_2 to approximately 2.0 eV, extending the optical

TABLE-5
COMPARATIVE DATA OF PHOTODEGRADATION OF VARIOUS ORGANIC POLLUTANTS REPORTED IN PREVIOUS STUDIES

Catalyst	Dye	Conc. of dye (mg/L)	Light source	Time (min)	Degradation (%)	Ref.
Bi-TiO_2	Alizarine	25	Vis	90	82	[32]
TiO_2/BMMs	Alizarine	25	Vis	180	93.6	[33]
Fe-TiO_2	Yellow XRG	100	Vis	480	37	[34]
Fe-TiO_2	Methyl orange	20	Vis	360	70	[35]
Pt-TiO_2	Methyl orange	20	UV	90	98	[36]
Cu-TiO_2	Methylene orange	10	Vis	45	100	[37]
Pd-TiO_2	Acid green 16	122	UV	60	80	[38]
Co-TiO_2	Alizarine	10	Vis	60	73.5	Present study
Co-TiO_2	Alizarine	10	UV	60	48.4	Present study
Co-TiO_2	Alizarine	10	Solar	60	63.4	Present study

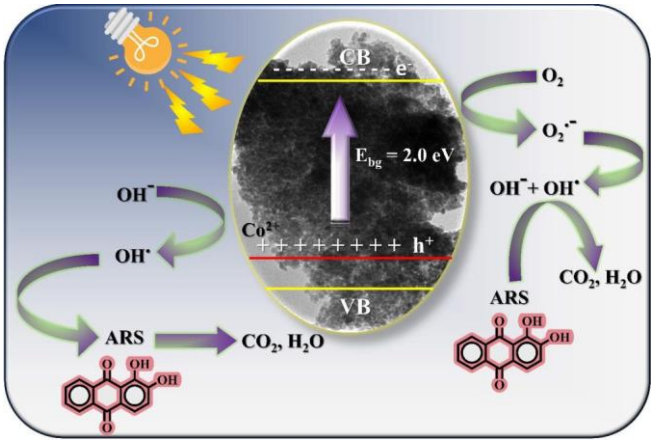

Fig. 7. The mechanism for photocatalytic degradation of alizarin red S (ARS) dye using Co-doped TiO_2

response toward the visible region. After 60 min of irradiation, ARS degradation reached 73.53% under UV light, 48.44% under visible light and 63.46% under solar irradiation. The visible-light degradation obtained with Co-doped TiO_2 represents an increase of approximately 48.4% relative to the negligible degradation observed with pristine TiO_2 under the same conditions, rather than a 25% increase. The enhanced photocatalytic response can be associated with the Co-induced modification of the electronic structure, extended light absorption and improved utilization of photogenerated charge carriers. The highly crystalline anatase phase identified by XRD, together with the nanoscale morphology and polycrystalline nature observed by TEM and SAED, supports the structural characteristics of the photocatalyst. The degradation kinetics followed a pseudo-first-order model, with apparent rate constants of 0.01819, 0.01073 and 0.01608 min^{-1} for UV, visible and solar irradiation, respectively. The substantial ARS degradation achieved under solar irradiation establishes Co-doped TiO_2 as a promising photocatalyst for solar-assisted treatment of dye-contaminated wastewater.

CONFLICT OF INTEREST

The authors declare that there is no conflict of interests regarding the publication of this article.

DECLARATION OF AI-ASSISTED TECHNOLOGIES

During the preparation of this manuscript, the authors used an AI-assisted tool(s) to improve the language and no data, results or scientific conclusions were generated by AI. All analyses, interpretations and conclusions are the authors' own. The authors reviewed and edited the content and take full responsibility for the published work.

REFERENCES

1. S. Dutta, S. Adhikary, S. Bhattacharya, S. Chatterjee, A. Chakraborty, D. Roy, D. Banerjee, A. Ganguly, S. Nanda and P. Rajak, *J. Environ. Manage.*, **353**, 120103 (2024); https://doi.org/10.1016/j.jenvman.2024.120103
2. D. Jiang, T.A. Otitoju, Y. Ouyang, N.F. Shoparwe, S. Wang, A. Zhang and S. Li, *Catalysts*, **11**, 1039 (2021); https://doi.org/10.3390/catal11091039
3. R. Daghrir, P. Drogui and D. Robert, *Ind. Eng. Chem. Res.*, **52**, 3581 (2013); https://doi.org/10.1021/ie303468t
4. P. Srivastava, S.A. Al-Obaidi, G. Webster, A.J. Weightman and D.J. Sapsford, *J. Environ. Manage.*, **317**, 115332 (2022); https://doi.org/10.1016/j.jenvman.2022.115332
5. T. Del Giacco, R. Germani, F. Saracino and M. Stradiotto, *J. Photochem. Photobiol. A: Chem.*, **332**, 546 (2017); https://doi.org/10.1016/j.jphotochem.2016.10.002
6. P. Jiang, W. Xiang, J. Kuang, W. Liu and W. Cao, *Solid State Sci.*, **46**, 27 (2015); https://doi.org/10.1016/j.solidstatesciences.2015.05.007
7. U. Jabeen, S.M. Shah and S.U. Khan, *Surf. Interfaces*, **6**, 40 (2017); https://doi.org/10.1016/j.surfin.2016.11.002
8. N. Klueb-arb, S. Chuangchote, K. Roongraung, N. Laosiripojana and T. Sagawa, *J. Sustain. Energy Environ.*, **9**, 11 (2018);
9. A. Ajmal, I. Majeed, R.N. Malik, H. Idriss and M.A. Nadeem, *RSC Adv.*, **4**, 37003 (2014); https://doi.org/10.1039/C4RA06658H
10. M.C. Collivignarelli, A. Abbà, M. Carnevale Miino and S. Damiani, *J. Environ. Manage.*, **236**, 727 (2019); https://doi.org/10.1016/j.jenvman.2018.11.094
11. M.D. Khan, A. Singh, M.Z. Khan, S. Tabraiz and J. Sheikh, *J. Water Process Eng.*, **53**, 103579 (2023); https://doi.org/10.1016/j.jwpe.2023.103579
12. D. Chen, Y. Cheng, N. Zhou, P. Chen, Y. Wang, K. Li, S. Huo, P. Cheng, P. Peng, R. Zhang, L. Wang, H. Liu, Y. Liu and R. Ruan, *J. Clean. Prod.*, **268**, 121725 (2020); https://doi.org/10.1016/j.jclepro.2020.121725
13. Y. Shi, J. Chen, S. Xiao, Y. Zhang and X. Zhou, *ACS ES&T Water*, **3**, 3449 (2023); https://doi.org/10.1021/acsestwater.3c00523
14. S.J. Armaković, M.M. Savanović and S. Armaković, *Catalysts*, **13**, 26 (2023); https://doi.org/10.3390/catal13010026
15. Y. Nosaka and A.Y. Nosaka, *Chem. Rev.*, **117**, 11302 (2017); https://doi.org/10.1021/acs.chemrev.7b00161
16. R. Acharya and P. Pani, *Mater. Today: Proc.*, **67**, 1276 (2022); https://doi.org/10.1016/j.matpr.2022.09.037
17. B. Roose, S. Pathak and U. Steiner, *Chem. Soc. Rev.*, **44**, 8326 (2015); https://doi.org/10.1039/C5CS00352K
18. B. Choudhury and A. Choudhury, *J. Luminescence*, **132**, 178 (2012); https://doi.org/10.1016/j.jlumin.2011.08.020
19. A. Safeen, K. Safeen, Zulfqar, W.H. Shah, Q. Zaman, K. Althubeiti, R. Ullah, S. Al Otaibi, N. Rahman, S. Iqbal, A. Khan, A. Khan and R. Khan, *RSC Adv.*, **12**, 15767 (2022); https://doi.org/10.1039/D2RA01948
20. R. Noonuruk and C. Wattanawikkam, *Curr. Appl. Sci. Technol.*, **20**, 43 (2020).
21. N. Thakur, N. Thakur, K. Kumar and A. Kumar, *Mater. Today: Proc.*, (2023); https://doi.org/10.1016/j.matpr.2023.01.253
22. P.W. Koh, L. Yuliati and S.L. Lee, *Malaysian J. Fundament. Appl. Sci.*, **11**, 126 (2015); https://doi.org/10.11113/mjfas.v11n3.382
23. M.M. Ahmad, S. Mushtaq, H.S. Al Qahtani, A. Sedky and M.W. Alam, *Crystals*, **11**, 1456 (2021); https://doi.org/10.3390/cryst11121456
24. P. Pardhi, K.L. Patle, K.S. Morla, J.D. Ekhe and A. Banerjee, *Energy Fuels*, **40**, 7458 (2026); https://doi.org/10.1021/acs.energyfuels.5c06238
25. K. Safeen, R. Ullah, A. Safeen, Zulfiqar, M. Kabeer, R. Khan, H. Ullah, A. Zaman, K. Shafique Ahmad, M.Z. Ullah Shah, H.O. Elansary, I. Mohamed Moussa, R. Casini and E.A. Mahmoud, *J. Saudi Chem. Soc.*, **27**, 101711 (2023); https://doi.org/10.1016/j.jscs.2023.101711
26. S. Akel, R. Boughaled, R. Dillert, M. El Azzouzi and D.W. Bahnemann, *Molecules*, **25**, 249 (2020); https://doi.org/10.3390/molecules25020249
27. C. Byrne, L. Moran, D. Hermosilla, N. Merayo, Á. Blanco, S. Rhatigan, S. Hinder, P. Ganguly, M. Nolan and S.C. Pillai, *Appl. Catal. B*, **246**, 266 (2019); https://doi.org/10.1016/j.apcatb.2019.01.058

28. Y. Wang, R. Zhang, J. Li, L. Li and S. Lin, *Nanoscale Res. Lett.*, **9**, 46 (2014); https://doi.org/10.1186/1556-276X-9-46
29. T. Umebayashi, T. Yamaki, H. Itoh and K. Asai, *J. Phys. Chem. Solids*, **63**, no. 10, pp. 1909 (2002); https://doi.org/10.1016/S0022-3697(02)00177-4
30. M. Saini, M. Kumar and T. Som, *Appl. Surf. Sci.*, **418**, 302 (2017); https://doi.org/10.1016/j.apsusc.2017.01.262
31. A. Hussain, A. Rauf, E. Ahmed, M. S. Khan, S. A. Mian and J. Jang, *Molecules*, **28**, 3252 (2023); https://doi.org/10.3390/molecules28073252
32. S. Sood, S.K. Mehta, A. Umar and S.K. Kansal, *New J. Chem.*, **38**, 3127 (2014); https://doi.org/10.1039/C4NJ00179F
33. A. Gul, J. Sun, R. Ullah, T. Munir and S. Bai, *ChemistrySelect*, **6**, 6816 (2021); https://doi.org/10.1002/slct.202100813
34. J. Zhu, W. Zheng, B. He, J. Zhang and M. Anpo, *J. Mol. Catal. Chem.*, **216**, 35 (2004); https://doi.org/10.1016/j.molcata.2004.01.008
35. T. Tong, J. Zhang, B. Tian, F. Chen and D. He, *J. Hazard. Mater.*, **155**, 572 (2008); https://doi.org/10.1016/j.jhazmat.2007.11.106
36. M. Huang, C. Xu, Z. Wu, Y. Huang, J. Lin and J. Wu, *Dyes Pigments*, **77**, 327 (2008); https://doi.org/10.1016/j.dyepig.2007.01.026
37. M. Hamadanian, A. Reisi-Vanani and A. Majedi, *Appl. Surf. Sci.*, **256**, 1837 (2010); https://doi.org/10.1016/j.apsusc.2009.10.016
38. S. Sakthivel, M.V. Shankar, M. Palanichamy, B. Arabindoo, D.W. Bahnemann and V. Murugesan, *Water Res.*, **38**, 3001 (2004); https://doi.org/10.1016/j.watres.2004.04.046
39. Y. Yu, H. Ming, D. He, J. Li, Y. Jin, H. Sun, M. Ahmad and X. Wang, *J. Environ. Chem. Eng.*, **11**, 111243 (2023); https://doi.org/10.1016/j.jece.2023.111243